





Landslide susceptibility: a statistically-based assessment on a depositional pyroclastic ramp

Franny G. MURILLO-GARCÍA^{1*}  <https://orcid.org/0000-0003-2064-4877>;  e-mail: fran.79v@gmail.com

Stefan STEGER²  <https://orcid.org/0000-0003-0886-5191>; e-mail: stefan.steger@eurac.edu

Irasema ALCÁNTARA-AYALA¹  <https://orcid.org/0000-0003-0794-1201>; e-mail: irasema@igg.unam.mx

*Corresponding author

¹ Institute of Geography, National Autonomous University of Mexico (UNAM), Circuito Exterior, Ciudad Universitaria, 04510, Coyoacán, Mexico City, Mexico

² Institute for Earth Observation, Eurac Research. Drususallee 1/Viale Druso 1, 39100 Bozen-Bolzano, Italy

Citation: Murillo-García FG, Steger S, Alcántara-Ayala I (2019) Landslide susceptibility: a statistically-based assessment on a depositional pyroclastic ramp. *Journal of Mountain Science* 16(3). <https://doi.org/10.1007/s11629-018-5225-6>

© Science Press, Institute of Mountain Hazards and Environment, CAS and Springer-Verlag GmbH Germany, part of Springer Nature 2019

Abstract: This study aimed to produce a high-quality landslide susceptibility map for Teziutlán municipality, a landslide-prone region in Mexico, which is characterised by a depositional pyroclastic ramp. The heterogeneous quality of available topographic information (i.e. higher resolution digital elevation model only for a sub-region) encouraged to confront modelling results based on two different study area delineations and two raster resolutions. Input data was based on the larger modelling region L15 (163 km²) and smaller S (70 km²; located inside L15) with an associated raster cell size of 15 m (region L15 and S15) and 5 m (region S5). The resulting three data sets (L15, S15 and S5) were included into three differently flexible modelling techniques (Generalized Linear Model - GLM, General Additive Model - GAM, Support Vector Machine -SVM) to produce nine landslide susceptibility models. Preceding variable selection was performed heuristically and supported by an exploratory data analysis. The final models were based on the explanatory variables slope angle, slope aspect, lithology, relative slope position, elevation, convergence index, distance to streams, distance to springs and topographic wetness index. The ability of the models to classify independent test data was

elaborated using a k-fold cross validation procedure and the AUROC (Area Under the Receiver Operating Characteristic) metric. In general, all produced landslide susceptibility maps depicted the hillslopes of the ravines, which cut the pyroclastic ramp, as prone to landsliding. The modelling results showed that predictive performances (i.e. AUROC values) slightly increased with an increasing flexibility of the applied modelling technique. Thus, SVM performed best, while the GAM outperformed the GLM. This tendency was most distinctive when modelling with the largest landslide sample size (i.e. data set L15; $n = 662$ landslides). Non-linear classifiers (GAMs, SVMs) performed slightly better when trained on the basis of lower raster resolution (data set S15) compared to the 5 m counterparts (data set S5). Highest predictive performance was obtained for the model based on data set L15 and the SVM classifier (median AUROC: 0.82). However, SVMs also indicated the highest degree of model overfitting. This study indicates that the decision to delineate a study area, the selection of a raster resolution as well as the chosen classification technique can affect varying aspects of subsequent modelling results. The results do not support the assumption that a higher raster resolution (i.e. a more detailed digital representation of the terrain) inevitably leads to better performing or geomorphically more plausible landslide

Received: 26-Sep-2018

Revised: 11-Nov-2018

Accepted: 20-Jan-2019

susceptibility maps.

Keywords: Landslide susceptibility; Pyroclastic ramp; Logistic regression; Generalized Additive Model; Support Vector Machine; Cross validation

Introduction

Landslide susceptibility can be defined as the spatial likelihood of landsliding due to a particular set of static environmental conditions (Guzzetti 2005). Susceptibility maps provide a spatial evaluation concerning the location of potential future slope instabilities and areas where landslides are not to be expected (Cardinali et al. 2002; Guzzetti et al. 1999, 2005). In general, landslide susceptibility can be elaborated using qualitative, semi-quantitative or quantitative approaches (Reichenbach et al. 2018). Qualitative approaches, where a domain expert determines the most susceptible zones, are considered subjective as the results are mainly founded on experience and knowledge of a person (van Westen et al. 1999; Chen et al. 2009; Chauhan et al. 2010). Quantitative analyses are either based on physical laws (e.g. infinite slope models) or on empirical rules (i.e. statistically-based classifiers) that allow the combination of available spatial environmental information (Fell et al. 2008). Despite the large number of published research in the field of quantitative landslide susceptibility modelling, there is still no encompassing agreement on which modelling approach to choose under which circumstances (Brabb 1984; van Westen et al. 1997; Guzzetti et al. 1999; Glade and Crozier 2005; Reichenbach et al. 2018).

In summary, statistically-based approaches built an empirical association between past landslide occurrences (and non-occurrences) and static environmental factors to elaborate typical landslide conditions. Resultant landslide susceptibility maps spatially depict the resultant classification rule in the form of a relative estimate on the propensity of spatial units to be affected by landslide susceptibility. The subsequent quantitative model validation primarily focuses on comparing the predicted susceptibility score with test data that was not applied to train the model (Chung and Fabbri 2003; Steger et al. 2016a).

Statistically-oriented classification techniques are especially valuable for larger areas, also because of their lower reliance on challenging to derive geotechnical information (Fell et al. 2008; Cascini 2008). During the last decade, a vast number of publications confronted modelling results obtained by different statistical classification techniques (Brenning 2005; Rossi et al. 2010; Goetz et al. 2011; Vorpahl et al. 2012; Pradhan 2013; Kavzoglu et al. 2014; Pourghasemi and Rahmati 2018). Other research focused on the effects of data properties on the reliability of subsequent landslide susceptibility maps concluding that the input data quality co-determines the final modelling results (Guzzetti et al. 2006; Cascini 2008; van Westen et al. 2008; Petschko et al. 2016; Steger et al. 2017; Zêzere et al. 2017).

According to literature, terrain derivatives extracted from Digital Elevation Models (DEMs) are regularly used in combination with thematic information as potential explanatory variables (Conforti et al. 2014). Commonly used terrain attributes include slope, aspect, elevation, slope curvature and diverse proxies for hydrological influences (Reichenbach et al. 2018).

Several publications emphasize that the quality and spatial resolution (i.e. pixel size) of the underlying topographic information (i.e. DEM) co-determines the final modelling results (Lee et al. 2004; Akgün and Bulut, 2007; Catani et al. 2013; Fressard et al. 2014; Palamakumbure et al. 2015; Schlögel et al. 2018). Catani et al. (2013) emphasized that the optimal input data configuration changes with the pre-selected spatial scale in a notable manner, while Legorreta-Paulín et al. (2010) and Trigila et al. (2015) highlighted that model performance generally improved with increasing resolution of input data. Palamakumbure et al. (2015) concluded that a 10m DEM resolution was the optimal choice for modelling landslide prone terrain within their study site. Yet, in some areas, particularly in less developed countries, high quality topographic information, as derived by Light Detection and Ranging (LiDAR), is rarely available (Deb et al. 2009; Althuwaynee et al. 2014; Romer and Ferentinou 2016).

The aim of this study was to produce a high-quality landslide susceptibility map for Teziutlán.

For this purpose, statistical-based landslide susceptibility modelling was performed. The objective was to confront modelling results based on different study area delineations (region L vs. S), different raster resolutions (5 m vs. 15 m) and differently flexible modelling algorithms in order to develop a suitable model for the study site with availability of heterogeneous data qualities. Thus, the presented research not only allowed insights into the effect of differently flexible classifiers on the modelling results, but also into the interplay between classification algorithms, study area delineation and modelling resolution. The

produced nine models were evaluated quantitatively (e.g. k-fold cross validation) and qualitatively (e.g. prediction pattern).

1 Study Area

Teziutlán municipality is located in the Sierra Norte of Puebla mountainous system, within the transition of the Sierra Madre Oriental and the Trans-Mexican Volcanic Belt physiographic provinces (Figure 1). The capital town of the municipality is also called Teziutlán and it is

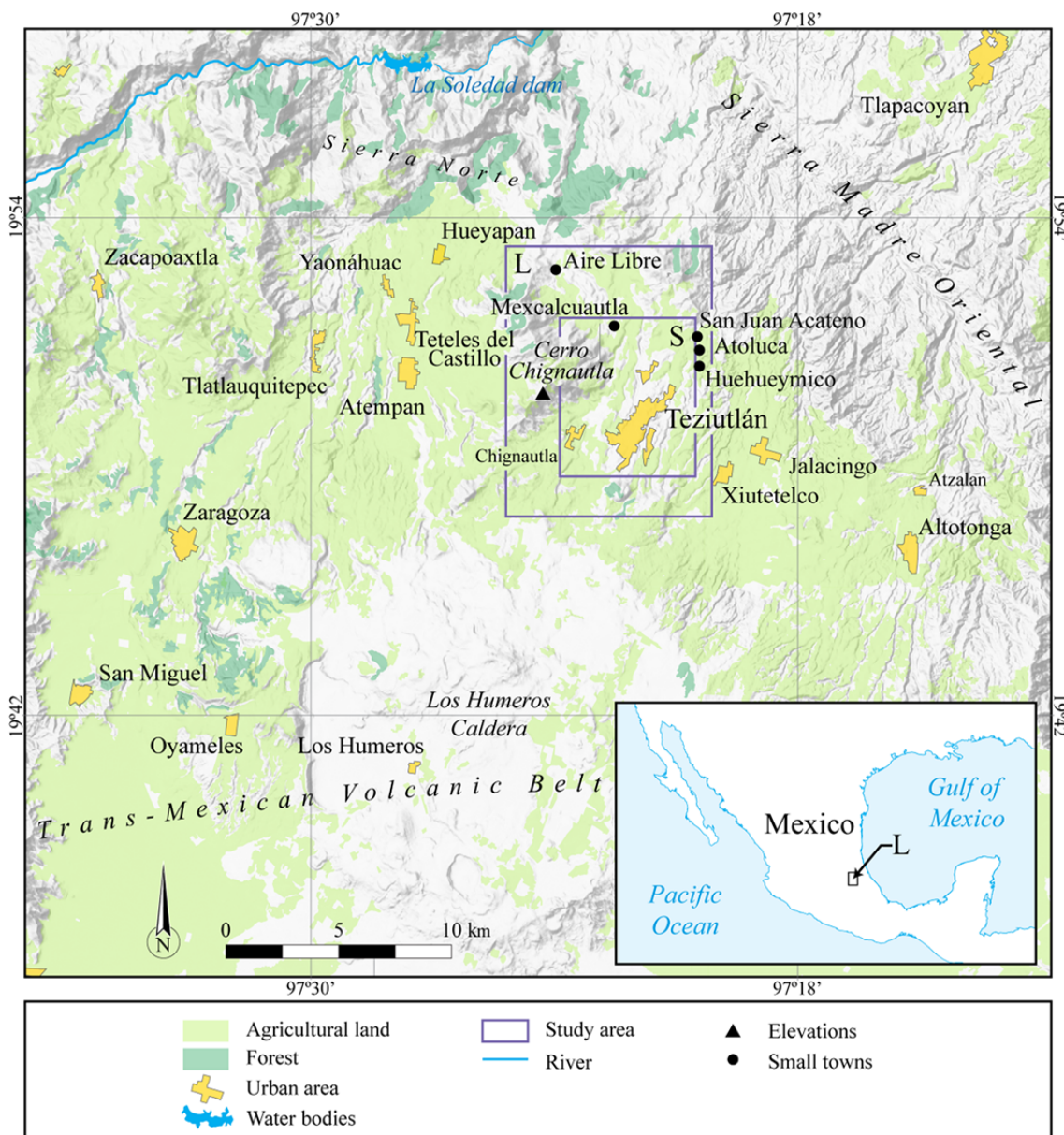


Figure 1 Location map. The analyses were based on two different study area delineations, L15 and S5. DEM resolution was 15 m for the data set L15, 5 m for S5 and 15 m for S15.

located on the top of a plateau formed by lava flows and pyroclastic materials from Los Humeros caldera volcano (LHVC), which is situated approximately 20 km to the South of Teziutlán town.

The climate can be described as warm temperate (range 12°C-22°C) and rainfall takes place all year long (precipitation ranges per year: 1100-3600 mm) (INEGI 2009). The main drainage of the area is oriented N-S and NE-SW and influenced by tectonic lineaments (Capra et al. 2003). The soils of the area are of volcanic origin and can predominantly assigned to the group of andosols (INEGI 2009). Human impact led to the tendency that the original vegetation (mountainous cloud forest) has been removed or replaced by grasslands, arable land and urban areas. Only at the north of the study area pine-oak woodlands are still present. The geology of Teziutlán (Figure 2) is linked directly to the activity of LHVC, one of the Pleistocene silica centres (Dávila-Harris and Carrasco-Núñez 2014). Among the eruptive products derived from LHVC that range from

basalt to high-silica rhyolite, the Xaltipan ignimbrite is the most significant deposit. Most of these deposits are non-welded material easily recognized as ash-pumice flow deposits. These pyroclastic flows filled low areas of the rugged pre-existing terrain covering a surface of circa 3500 km² (Ferriz and Mahood 1984) and formed ramps. Further details on the geological context of the area can be found in Murillo-García and Alcántara-Ayala (2017).

2 Materials and Methods

2.1 Landslide inventory and landslide absences

The landslide inventory used within this study consists of 662 landslides of the slide-type movement (Varnes and IAEG 1984). Four different archives of aerial photographs served as the basis for the visual identification of geomorphic landslide features: (i) the archive of the National

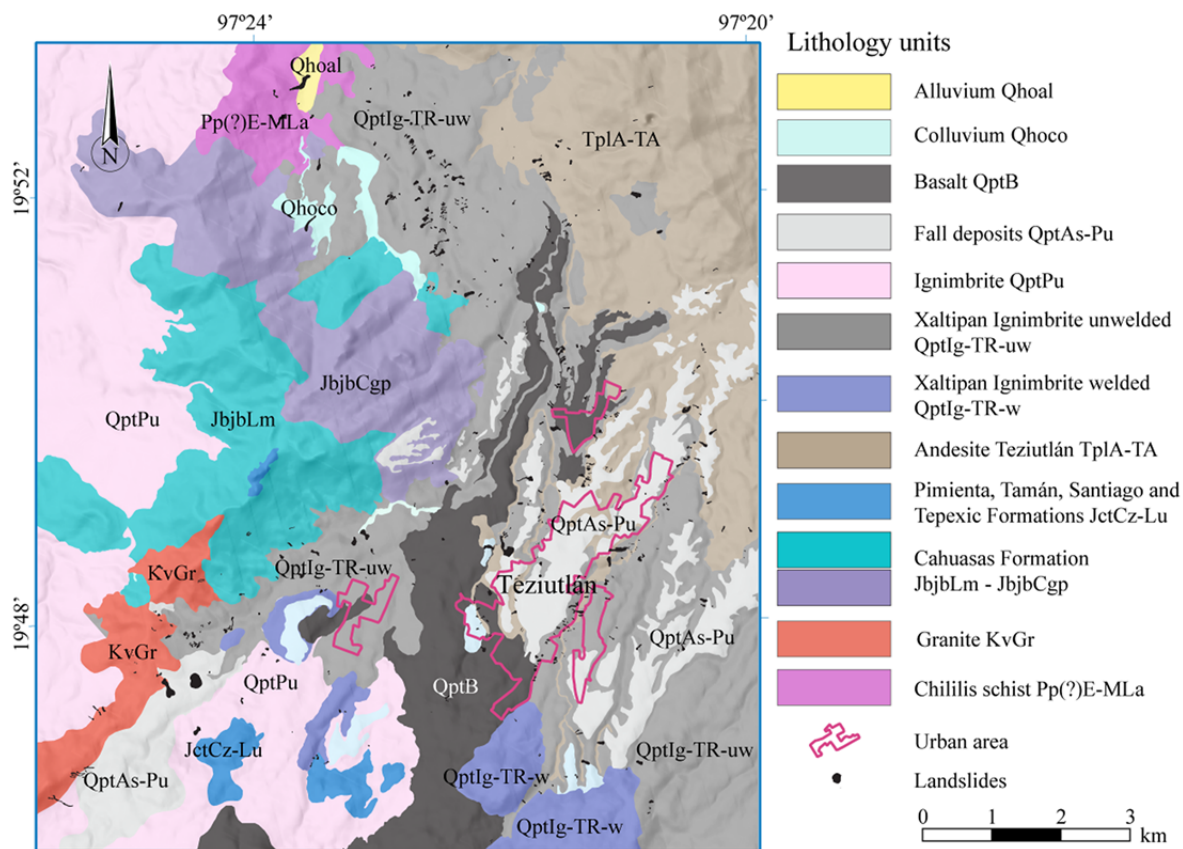


Figure 2 Lithology map with the rock units (modified from Salinas-Rodríguez and Castillo-Reynoso 2011) Sedimentary rocks were joined on a single class. The same applied for the Andesite Teziutlán and granite layers.

Institute of Statistics and Geography (INEGI), (ii) the archive of ICA Foundation (private entity), (iii) the library of the Geography Institute of the National University of Mexico (UNAM), and the archive of the National Centre for Disaster Prevention (CENAPRED). In summary, stereo-pairs of aerial photographs for the years 1942, 1956, 1974, 1978, 1980, 1991, 1999 and 2007 as well as very high resolution satellite images from the period 1999 to 2015 were adopted. Additional field surveys were carried out to cross-check the previously mapped landslides. More details on the landslide inventory can be found in [Murillo-García and Alcántara-Ayala \(2017\)](#).

For modelling, landslide occurrences were represented by one point per mapped landslide initiation zone as recommended by several previous investigations to avoid a weighting for landslide magnitude and to reduce the impact of spatial autocorrelation ([Atkinson and Massari 1998](#); [van den Eeckhaut et al. 2006](#); [Qi et al. 2010](#); [Gorum et al. 2011](#); [Petschko et al. 2014](#); [Goetz et al. 2015](#)). Landslide absence locations related to a random sample of points outside digitized landslide bodies. The final binary response variables consisted of an identical number of landslide presence and absence observations (1:1 sampling) ([Heckmann et al. 2014](#); [Regmi et al. 2014](#); [Goetz et al. 2015](#); [Steger et al. 2016a](#)). [Hussin et al. \(2016\)](#) analysed the effects of different sampling strategies for a grid-based susceptibility modelling and concluded that in some cases, even a minor proportion of 1:1 could be sufficient to obtain meaningful landslide susceptibility models.

2.2 Study area definition and environmental variables

The topographic variables of this study relate to two DEMs of varying quality. The coarser scaled DEM (i.e. 15 m) was constructed by using photogrammetric techniques ([INEGI 2013a](#)) whereas the higher resolved DEM (i.e. 5 m) was based on an aerial LiDAR campaign (flight on January 20, 2010) ([INEGI 2013b](#)). Two different study area delineations (Larger L and smaller S) were defined because only the 15 m DEM covers the entire study area ([Figure 1](#)). In detail, the entire study area extends over 163 km² (region L15) while the sub-region covers 70.3 km² (region S5).

Summarizing, region L is larger and region S represent a sub-region of L ([Figure 1](#)). Data set L15 relates to the 163 km² large region, 662 mapped landslides and a DEM resolution of 15 m. The data set S5 relates to the mentioned sub-region (70.3 km²), 449 landslides and the 5 m DEM ([Table 1](#)). The third data set, namely S15, covers the same extension as region S5 (70.3 km²), but is based on a coarser DEM resolution (i.e. 15 m).

Table 1 Study area extent, pixel size and number of landslides (see also [Figure 1](#)).

Data set	Extent (km ²)	Pixel size (m)	Landslides
L15	163	15	662
S5	70.3	5	449
S15	70.3	15	449

Comparisons of the models based on the data set L15 and S15 allowed to scrutinize the effect of study area delineation by keeping the modelling resolution constant (i.e. 15 m) ([Gordo et al. 2017](#); [Steger and Glade 2017](#)). The influence of raster resolution was elaborated by confronting modelling results based on the identical study area delineation, but on different modelling resolutions (S5: 5 m vs. S15: 15 m).

Within this study, candidates of frequently used explanatory variables were analysed prior to select or dismiss them for further analyses ([Table 2](#)). The two different DEMs served as a basis to derive slope angle, slope aspect, general curvature, plan curvature, profile curvature, Topographic Wetness Index (TWI) ([Beven and Kirkby 1979](#)), Stream Power index (SPI) ([Moore et al. 1991](#)), Convergence Index (CI) ([Olaya 2004](#)), relative slope position (RSP) and catchment area within the SAGA GIS software ([Conrad 2006](#)). Furthermore, a reclassified lithology layer as well as the variables vertical distance to streams (VDTCHN), distance to streams, and distance to springs were produced.

Slope angle is the most frequently used predictor in statistical landslide susceptibility modelling and commonly considered as the main static explanatory variable of landslide occurrence ([Costanzo et al. 2012](#); [Reichenbach et al. 2018](#)). Information on the altitude of an area, as directly represented by the DEM, can be seen as a proxy for altitude-dependent variation in weathering conditions ([Costanzo et al. 2012](#)). The general morphometric form of an area may be linked to the variability in overland water flow and soil moisture

Table 2 Data summary by scale, type and producer

Potential explanatory variables		Type	Producer
Topographic	Slope	Numerical (degrees)	SAGA GIS
	Elevation	Numerical (meters above sea level)	INEGI
	Aspect	Categorical: North, East, South and West.	SAGA GIS
	General Curvature		
	Plan Curvature	Numerical (dimensionless)	SAGA GIS
	Profile Curvature		
	Relative slope position	Numerical (0-1)	SAGA GIS
Hydrological	Convergence index	Numerical (percent)	SAGA GIS
	Vertical distance to streams	Numerical (meters)	SAGA GIS
	Catchment area	Numerical (square meters)	SAGA GIS
	Topographic Wetness Index	Numerical (dimensionless)	SAGA GIS
	Stream Power Index	Numerical (dimensionless)	SAGA GIS
	Distance to springs	Numerical (meters)	SAGA GIS and field surveys.
Geological	Distance to streams	Numerical (meters)	SAGA GIS
	Lithology units	Categorical (rock type) (1) Basalt-andesite (2) Sedimentary hard rock (conglomerate, limestone, Limonite) (3) Tertiary igneous hard rock (andesite-basalt from Teziutlán formation, and granite) (4) Falls deposits (ash-pumice-lapilli), colluviums and alluvium (5) Pumice flow unwelded (QptPu) (6) Pumice flow unwelded (QptlgTr-uw) (7) Pumice flow welded (QptlgTr-w) (8) Schist*	SGM and field surveys.

Notes: *Schist rock unit is not present at 5 m extension area and consequently not included in the S5 and S15 models. INEGI is the acronym for National Institute of Geography and Statistics of Mexico, and SGM is National Geological Service of Mexico.

conditions that in turn may influence soil properties. Proxys for hydrological influences are frequently represented by second order DEM derivatives, such as curvature, CI (Ayalew et al. 2004; Olaya 2004; San 2014) or by variables such as the TWI or the catchment area (Dahal et al. 2008; Costanzo et al. 2012; Catani et al. 2013). Slope aspect refers to the orientation of a hillslope and may represent effects related to the varying intensities of insolation (Catani et al. 2013; Guzzetti et al. 1999).

The Euclidean distance to streams and the vertical distance to channels describe the proximity or remoteness to potential landslide influencing linear features. The streams of the study area have incised deep steep valleys and ravines into the pyroclastic ramp deposits. SPI represents an approximation of the erosive power and may be associated with potential slope undercutting. Field observations suggest that landslides are frequently at the top of these depth ravines. Hence, RSP can be a suitable explanatory variable as it indicates the

relative position of each cell at a hillslope (e.g. ridge, middle slope, valley). Field surveys suggested an increasing landslide occurrence in closer proximity to springs. Besides higher water availability, locations closer to springs could also be indicative of the existence of faults covered by pyroclastic deposits. Thus, the proximity variable distance to springs was included as a potential variable candidate.

Lithology is a frequent proxy for the parent material. Within this study, some lithology classes were merged into a unique class in case of similar geotechnical properties (Table 2). The lithology layer is based on a 1:50,000 geologic map published by the National Geological Service of Mexico (Servicio Geológico Mexicano, SGM) (Salinas-Rodríguez and Castillo-Reynoso 2011).

Petschko et al. (2014) pointed out that land cover may often not be considered as static in time and therefore not suitable to link with historical landslide data (i.e. unknown temporal occurrence). In some cases, specific land cover units can even be

linked to a systematic under- or overrepresentation of mapped landslide information (e.g. incomplete mapping in forested areas). An inclusion of land cover as a variable may therefore lead to biased statistical relationships (Steger et al. 2017). Since both arguments may be valid for the present study, the conducted analysis did not consider currently observable land cover conditions.

2.3 Exploratory data analysis and variable selection

The selection of explanatory variables is an important step in landslide susceptibility modelling (Costanzo et al. 2012). Within this study, variable selection was performed heuristically, supported by an exploratory data analysis.

An initial evaluation of the Individual Classification Power (ICP) revealed the ability of each variable to discriminate observations of the binary response. The ICP relates to model predictions (score between 0-1) which are based on classifiers trained separately for each single variable (i.e. one model per predictor). The Area Under the Receiver Operating Characteristic (AUROC) curve (Hosmer and Lemeshow 2000) was used as a metric to evaluate the ICP (Zweig and Campbell 1993; Goetz et al. 2015). In summary, the AUROC curve plots all positive true rates (sensitivity) against associated false positive rates (1 – specificity) for each possible probability

threshold. The presented AUROC scores are based on the R package “ROCR” (Sing et al. 2009). An AUROC of 1 depicts that the respective single-variable model enabled a perfect separation of landslide presences and absences while a value of 0.5 points to a random classification. In the case two or more variables represented a similar landslide influencing factor (i.e. curvature and convergence index), we opted to include only one in order to decrease redundancies and ensure a parsimonious and interpretable model. In this context, also the ICP was taken into account for variable selection/rejection (i.e. the respective variable had a lower mean ICP than a variable that stands for a similar landslide explanatory variable). GLM regression coefficients provided insights into the direction of modelled associations between landslide occurrence and single continuously scaled predictor variables from a single-predictor perspective. Positive trends (i.e. “+” in Table 3) indicated that the modelled likelihood of landslide occurrence increases with an increasing predictor value (e.g. increasing slope angles) while negative trend (i.e. “-“ in Table 3) depicts the opposite tendency. Variables that showed a geomorphically unreasonable association to landslide occurrence were rejected from subsequent modelling.

2.4 Classification and model validation

Three different binary soft classification

Table 3 Results of individual classification power (AUROC values). +/-, trend of association based on regression coefficients. GLM, logistic regression; GAM, general additive model regression; SVM, support vector machine; RSP, relative slope position index; SPI, stream power index; TWI, topographic wetness index; VDTCHN, vertical distance to channel.

Variables	L15 (15 m)				S15 (15 m)				S5 (5 m)			
	GLM	GAM	SVM	Trend	GLM	GAM	SVM	Trend	GLM	GAM	SVM	Trend
Slope	0.538	0.579	0.607	+	0.504	0.578	0.621	+	0.643	0.643	0.658	+
Lithology	0.717	0.717	0.659		0.710	0.710	0.744		0.694	0.694	0.661	
Aspect	0.556	0.556	0.552		0.557	0.555	0.590		0.547	0.547	0.540	
Catchment area	0.484	0.514	0.543	+	0.506	0.560	0.515	-	0.501	0.513	0.495	+
CI	0.542	0.542	0.583	-	0.550	0.550	0.629	-	0.595	0.597	0.609	-
Curvature	0.499	0.522	0.537	-	0.490	0.509	0.55	+	0.526	0.546	0.59	-
Elevation	0.620	0.633	0.675	-	0.672	0.672	0.694	-	0.672	0.672	0.703	-
Plan curvature	0.490	0.537	0.564	+	0.517	0.517	0.571	-	0.554	0.554	0.567	+
Profile curvature	0.504	0.544	0.428	+	0.501	0.531	0.581	-	0.497	0.612	0.619	+
Distance to streams	0.595	0.595	0.625	+	0.64	0.64	0.671	-	0.579	0.580	0.620	+
RSP	0.593	0.612	0.611	-	0.633	0.633	0.646	-	0.601	0.628	0.625	-
SPI	0.506	0.515	0.525	-	0.518	0.534	0.542	+	0.414	0.596	0.581	-
Distance to spring	0.521	0.607	0.62	-	0.540	0.564	0.644	+	0.549	0.595	0.593	+
TWI	0.525	0.548	0.595	+	0.507	0.545	0.594	-	0.564	0.57	0.571	+
VDTCHN	0.580	0.580	0.589	-	0.646	0.646	0.658	-	0.533	0.558	0.553	+

techniques were used to model landslide susceptibility for the three data sets (L15, S5 and S15) leading to nine models in total. For this purpose, we opted for three differently flexible classifiers in order to find out if a more flexible algorithm would favour more reliable spatial predictions for the study site. Thus, we confronted classifiers based on a linear structure (i.e. Generalized Linear Model; GLM) with a moderately flexible semi-parametric algorithm (i.e. Generalized Additive Model; GAM) and a comparably flexible machine learning technique (i.e. Support Vector Machine; SVM).

GLM are based on a linear model structure and allow tackling two-class classification problems using a combination of scalar and categorical predictors. A GLM with a logistic link function (also referred to as binary logistic regression) is the most frequently used approach to model landslide susceptibility (Brenning 2005; Goetz et al. 2015; Reichenbach et al. 2018). The presented GLMs are based the R package “stats” (R Core Team 2016).

GAMs are semi-parametric extensions of GLMs (Hastie and Tibshirani 1986). GAMs are more flexible than GLMs and allow to account for non-linear relationships between the binary response and scalar predictor variables by applying empirically fitted smoothing functions (Hastie and Tibshirani 1990; Wood 2006). Several studies highlight that GAMs are suitable for mapping landslide-prone terrain (Park and Chi 2008; Brenning 2008; Goetz et al. 2011; Vorpahl et al. 2012; Petschko et al. 2013; Goetz et al. 2015; Youssef et al. 2015; Steger et al. 2016a). The GAMs were fitted using the “gam” R package (Hastie 2009).

Machine learning algorithms are usually more flexible than parametric or semi-parametric approaches and frequently applied for pattern recognition and classification. SVMs are popular to delineate landslide susceptibility while producing coherent spatial prediction patterns (Goetz et al. 2015; Steger et al. 2016a). A SVM is a maximum-margin classifier that enables non-linear discrimination between classes (e.g. landslide presence and absence) by transforming explanatory variables (i.e. the features) into a higher-dimensional feature space (Vapnik 1998; Hong et al. 2015). Within this higher dimensional

feature space, data points can be separated linearly using a hyperplane whose position maximizes the “margin” between the observations (Kotsiantis 2007). SVM hyperparameter tuning (C and sigma) was conducted via internal cross validation using a systematic grid search. SVMs were based on the R package “kernlab” (Karatzoglou et al. 2004) while parameter tuning was based on “mlr” (Bischl et al. 2016).

Modelling results obtained by GLMs, GAMs and SVMs were transferred to each pixel of the study area to spatially predict landslide-prone areas. The final maps were then visualized by classifying the obtained susceptibility scores into quintiles in Quantum GIS (QGIS Development Team 2009) to ensure a systematic visual comparability (Hussin et al. 2016). The classes were grouped into very low (saturated green colour), low (clear green colour), medium (yellow colour), high (orange colour), and very high (red) likelihood of landslide occurrence.

The capability of a landslide susceptibility model to “foresee” landsliding can be estimated by confronting predicted susceptibility scores with model independent test data (i.e. predictive capability) (Chung et al. 1995). Modelling results were evaluated by confronting the obtained classification rule (i.e. spatially predicted susceptibility scores) with previously sampled landslide presence/absence data via the AUROC. The elaboration of the predictive capability requires a splitting of the available data into training and test data. Performance estimates that are based on multiple partitions of training and test sets are less dependent on (random) variability associated with specific data partitions and enable to estimate the robustness of calculated metrics (e.g. via the interquartile range). For this study, data partitioning was based on a k-fold cross validation procedure implemented in the R package “sperrorest” (Brenning 2012). Each of the nine models has been evaluated by repeatedly splitting the initial data into multiple training and test sets. More precisely, the presented performance estimates (i.e. AUROCs) are based on 50 repetitions and 10 folds per repetition leading to 500 AUROCs for each of the nine models. More details on k-fold cross validation in the context of landslide susceptibility modelling can be found in Steger et al. (2016b). The inter-quartile range (IQR)

of obtained AUROCs provided insights into predictive performance variabilities (i.e. ~ uncertainties). Lower IQR indicates robust model performances and vice versa (Goetz et al. 2015). Additionally, an estimate on the degree of model overfitting was obtained by confronting fitting and predictive performances (i.e. median training set AUROC minus median test set AUROC).

3 Results

3.1 Variable selection

The results of the initial exploratory data analysis (Table 3) eased to select a common set of explanatory variables for subsequent statistical modelling. The results depict that the widely used predictor slope angle showed a positive relationship (trend) to landslide occurrence within all single-predictor GLMs and an ICP of > 0.64 for all classifiers at a resolution of 5 m. At 15 m resolution, the ICP for the predictor slope angle was < 0.63 for the SVM classifier and < 0.6 for the parametric and semiparametric models (GLM, GAM). GLMs pointed to negative trend between landslide occurrence and the elevation of the area with ICPs between 0.62 (GLM, data set L15) and 0.70 (SVM, data set S5). The topographic variables aspect and TWI showed maximum ICPs of 0.59 (SVM, data set S15) and 0.595 (SVM, data set L15) respectively. The ICP associated with the RSP was > 0.59 and < 0.65 while the associated relationship was constantly estimated to be negative (lower slope positions are more likely affected by landsliding). Comparing identical data set and classifier combinations (e.g. SVM, data set L15), RSP constantly showed higher ICPs than the other variable which relates to the relative hillslope position (Vdtchn). Thus, RSP was favoured over VDTCHN for subsequent modelling. The proximity variables, distance to streams and distance to spring were associated with ICPs > 0.57 and > 0.52 , respectively. We opted to dismiss the SPI variable due to its conceptual similarity with the distance to stream layer and low ICP values.

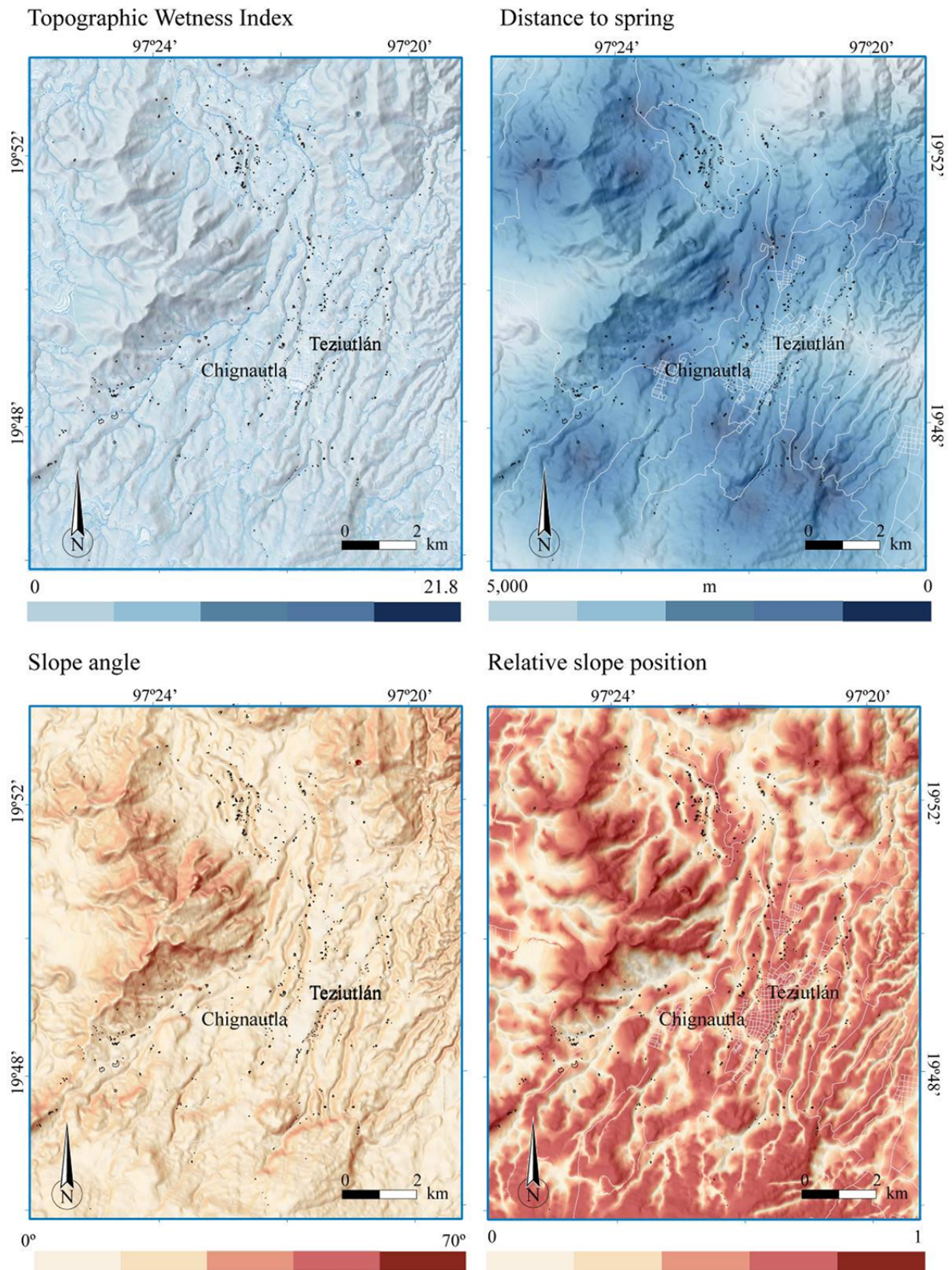
The curvature variables (general, plan and profile curvature), depicted contradictory trends in the estimated direction of association from one 15 m data set (L15) to the other (S15). Only the CI variable constantly depicted concave shaped areas

as more likely affected by landslide occurrence among all data sets. Also due to its comparably high ICP values (compared with the curvature variables), CI was favoured for successive modelling. The parametric and semi-parametric models (GLM, GAM) trained with the categorical variable lithology revealed particularly high ICPs of > 0.71 for low raster resolutions (i.e. 15 m) and > 0.69 for the 5 m models. The holistic interpretation of the previously described explanatory variables, in combination with experiences made during extensive field trips, led to the selection of the following predictor combination: slope angle, aspect, lithology, RSP, elevation, CI, distance to streams, distance to springs and TWI (Figure 3).

3.2 Model evaluation

Median AUROC scores (Figure 4) calculated on the basis of k-fold cross validation for all multiple variable models revealed an acceptable to excellent discrimination of model independent test cases (i.e. predictive performance) according the general rules of Hosmer and Lemeshow (2000). Predictive performance scores were > 0.76 and < 0.81 . A confrontation of classification techniques highlights that SVMs persistently outperformed the GLMs and GAMs produced with identical input data sets. In this context, GAMs performed second best while GLMs performed worst from a predictive performance point of view. Surprisingly, no substantial systematic difference in model performance was observed when confronting models generated on the basis of different data sets (L15 vs. S5 vs. S15; colours in Figure 4). Median AUROCs associated with the GLMs were slightly higher for the data set S15 (0.782) in comparison to L15 (0.759) and S5 (0.781). All GAMs performed equally well with median test set AUROCs > 0.779 and < 0.791 . SVMs performed better for L15 (0.817) than for S15 (0.791) and worst for the higher resolution data set S5 (0.794).

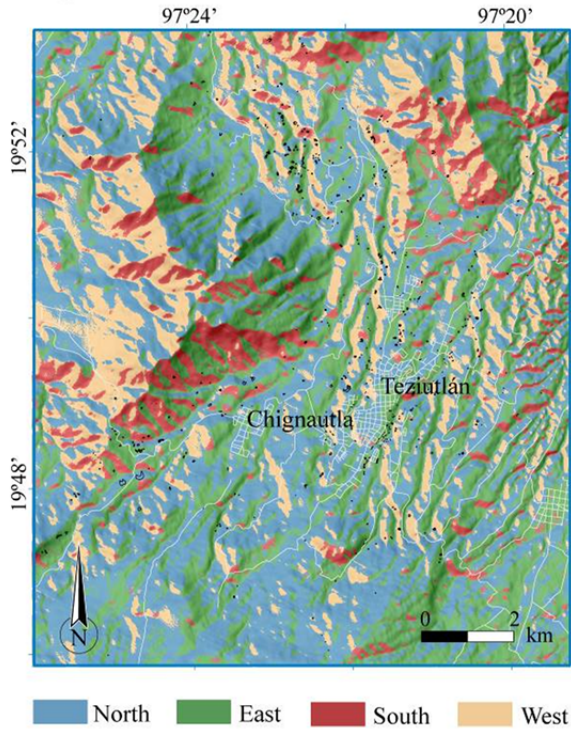
The box plot sizes (i.e. the vertical distance between the 1st and the 3rd quartile in Figure 4) can be interpreted as an indicator of prediction performance variability, i.e. uncertainty. In this context, all nine models showed rather similar variability in predictive performance uncertainty with IQRs ranging from 0.0506 (SVM, L15) to < 0.0670 (SVM, S5).



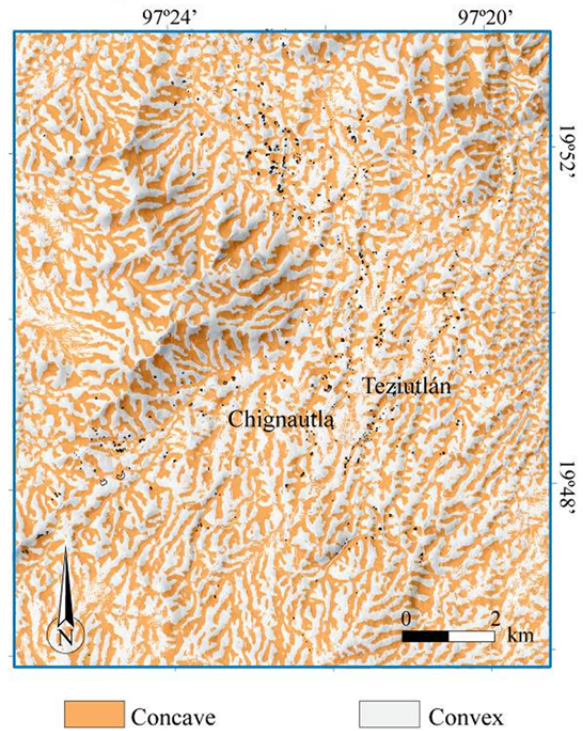
☉ Landslides initiation areas

Figure 3 Visual impression of selected explanatory variables (lithology is shown in Figure 2). Convergence index (here visualized according two classes) was included as continuously scale variable. TWI, Topographic Wetness Index; RSP, Relative slope position. (-To be continued-)

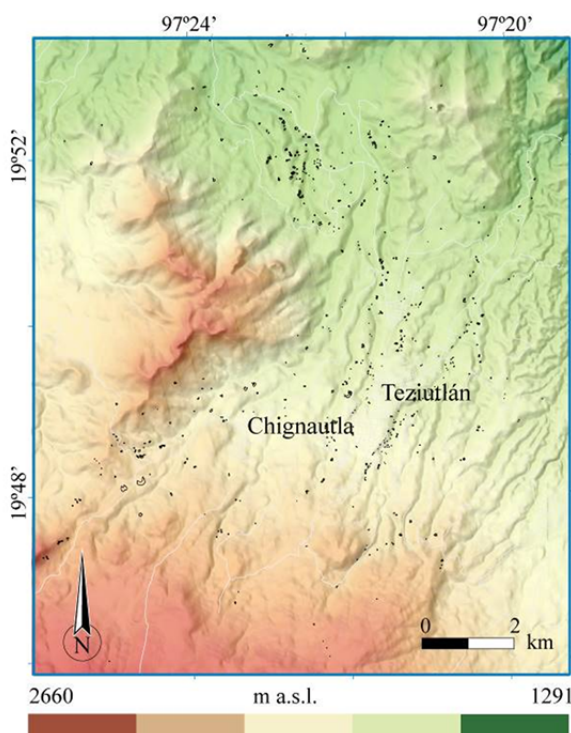
(-continued-)
Aspect



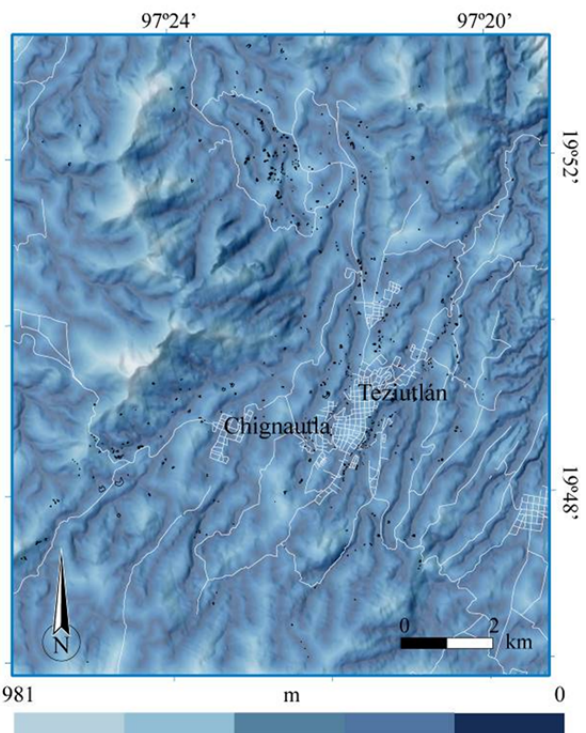
Convergence index



Elevation



Distance to rivers



☉ Landslides initiation areas

Figure 3 Visual impression of selected explanatory variables (lithology is shown in [Figure 2](#)). Convergence index (here visualized according two classes) was included as continuously scale variable. TWI, Topographic Wetness Index; RSP, Relative slope position.

The confrontation of obtained fitting performance scores (training data) and predictive performances (test data) allowed to gain insights into the degree of model overfitting (yellow triangles and right y axis in Figure 4). This analysis revealed that the most flexible and quantitatively best performing (i.e. predictive performance) classifier, namely SVM, exhibited the highest degree of model overfitting. The less flexible models, GLM and GAM, depicted a considerably lower tendency to “overlearn” the training data. In numbers, the discrepancy between median training and test AUROCs for the SVMs were 0.053 (L15), 0.060 (S15) and 0.063 (S5) while GLMs and the GAMs were associated with values from 0.019 to 0.026.

3.3 Susceptibility maps

The spatial prediction patterns associated with all landslide susceptibility maps are exemplarily depicted within Figure 5 for a landslide prone area. The superimposed landslide initiation zones and buildings outlines allow a visual confrontation with estimated susceptibility scores and provide a first impression of the relative exposedness of building infrastructure to landslide occurrence. The examples also highlight that the produced maps show a general spatial agreement of larger predicted susceptibility patterns. However, a more detailed evaluation also reveals some differences

between the maps because of different raster resolutions, classification algorithms and study area delineations.

The more detailed representation of topographic detail within all models based on the data set S5 is also reflected by a locally more differentiated pattern of predicted susceptibility scores. However, even if the respective maps may give rise to the impression of more detailed modelling results, associated predictive performances (Figure 4) did not provide quantitative evidence for a higher ability of the models to “foresee” future landsliding. The comparably high influence of lithological differences on the models based on GLM and GAM was reflected by abrupt changes in predicted landslide susceptibility within the southwest portion of the area, where sedimentary rocks are located next to the ignimbrite unit. The area characterized by sedimentary rocks (Chignautla hill) was estimated to be relatively unsusceptible to landsliding. In contrast, the maps based on SVM seemed to be less influenced by this categorical variable, but more reliant on topographical predictors (Figure 6). The observed higher portion of areas where very high and very low susceptibility values were situated in close proximity to each other went frequently hand in hand with abrupt changes in the topographical data, which is also influenced by the applied modelling resolution (i.e. smoother topography in case of lower resolution).

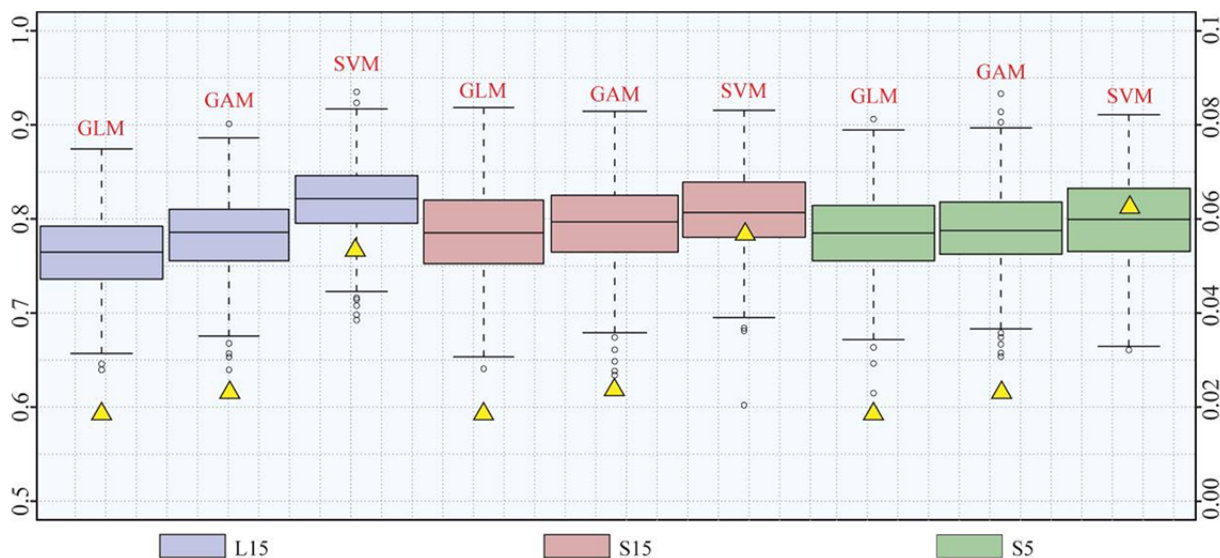


Figure 4 Box plots of k-fold cross validation based AUROC scores for all nine models. Left y axis shows AUROC scores, right y axis and yellow triangles indicates the degree of model overfitting (difference between median test set AUROC and training set AUROC).

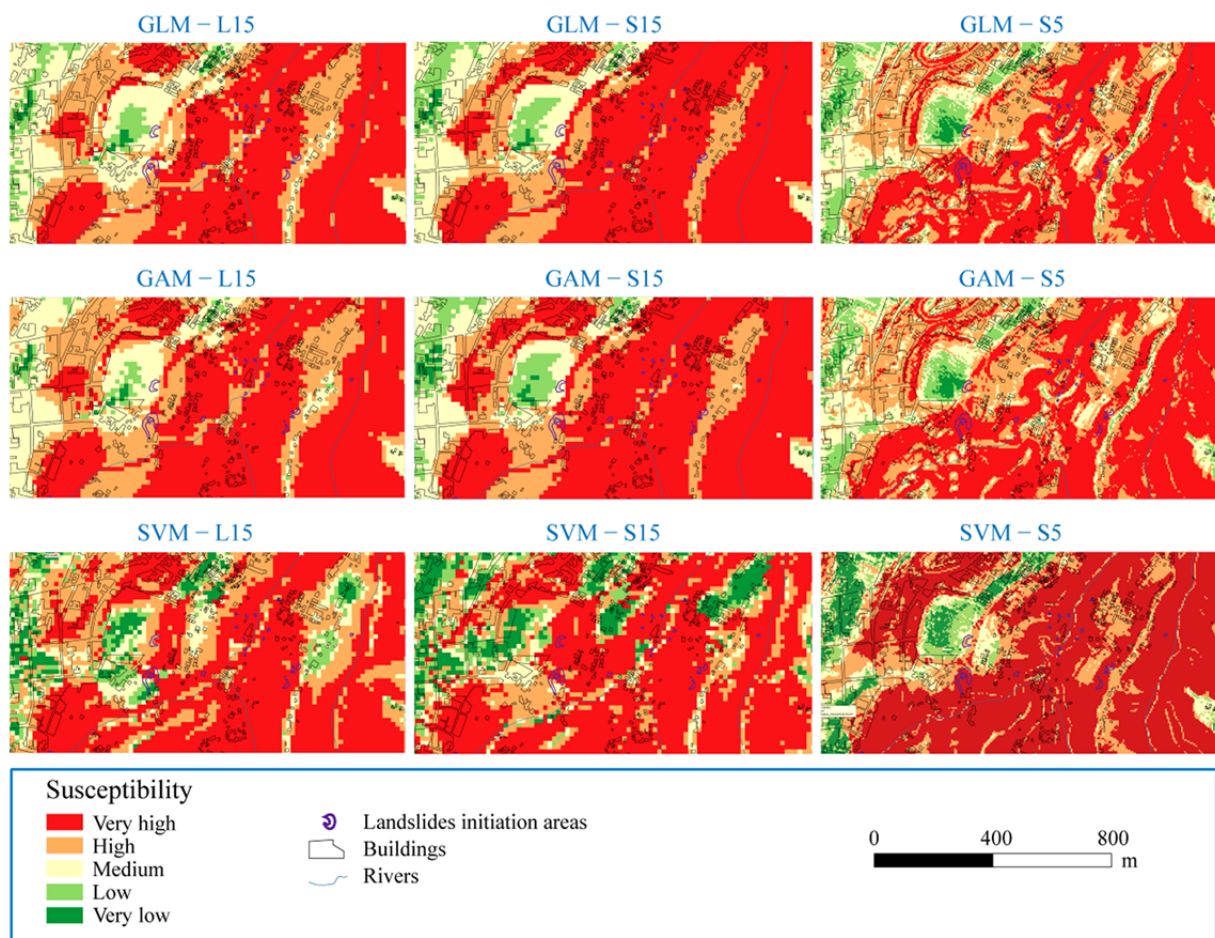


Figure 5 Classified (quintiles) landslide susceptibility maps at La Aurora neighbourhood.

4 Discussion

One aim of this study was to make effective use of available data on landslide occurrence and environmental data sets and to explore state-of-the-art modelling procedures in order to achieve a meaningful assessment of landslide-prone terrain. However, also within this study, the utilized data sets cannot be considered perfect. The complexity of the phenomenon under study, the spatially varying persistence of geomorphic landslide features and the limitations inherent in the adopted landslide mapping procedure (see section 2.4) inevitably influenced the spatial representativeness and accuracy of applied landslide information (Guzzetti et al. 1999; Glade and Crozier 2005; van Westen et al. 2008; Che et al. 2012).

It is supposed that the resulting limitations of landslide inventory data also affected the presented landslide susceptibility assessment (Ardizzone et al.

2002; Fressard et al. 2014). The influence of minor to medium positional errors of landslide data is expected to decrease with a coarser modelling resolution (Steger et al. 2016b). This is another argument why the utilization of larger cell sizes (in our case 15 m instead of 5 m) might not necessarily favor less meaningful analysis results. In fact, also obtained predictive performances did not reflect a superior ability of the 5 m models to predict out-of-model landslide observations. The present study highlighted that finding an optimal pixel resolution for landslide susceptibility modelling is not a trivial task. It contributes to previous research, which showed that higher DEM resolutions do not necessarily improve subsequent modelling results (Lee et al. 2004; Catani et al. 2013; Legorreta-Paulín et al. 2010; Palamakumbure et al. 2015; Trigila et al. 2015). A geomorphology oriented interpretation of the results indicated that emphasis should be placed to find a balance between topographic detail (i.e. DEM) and coarser

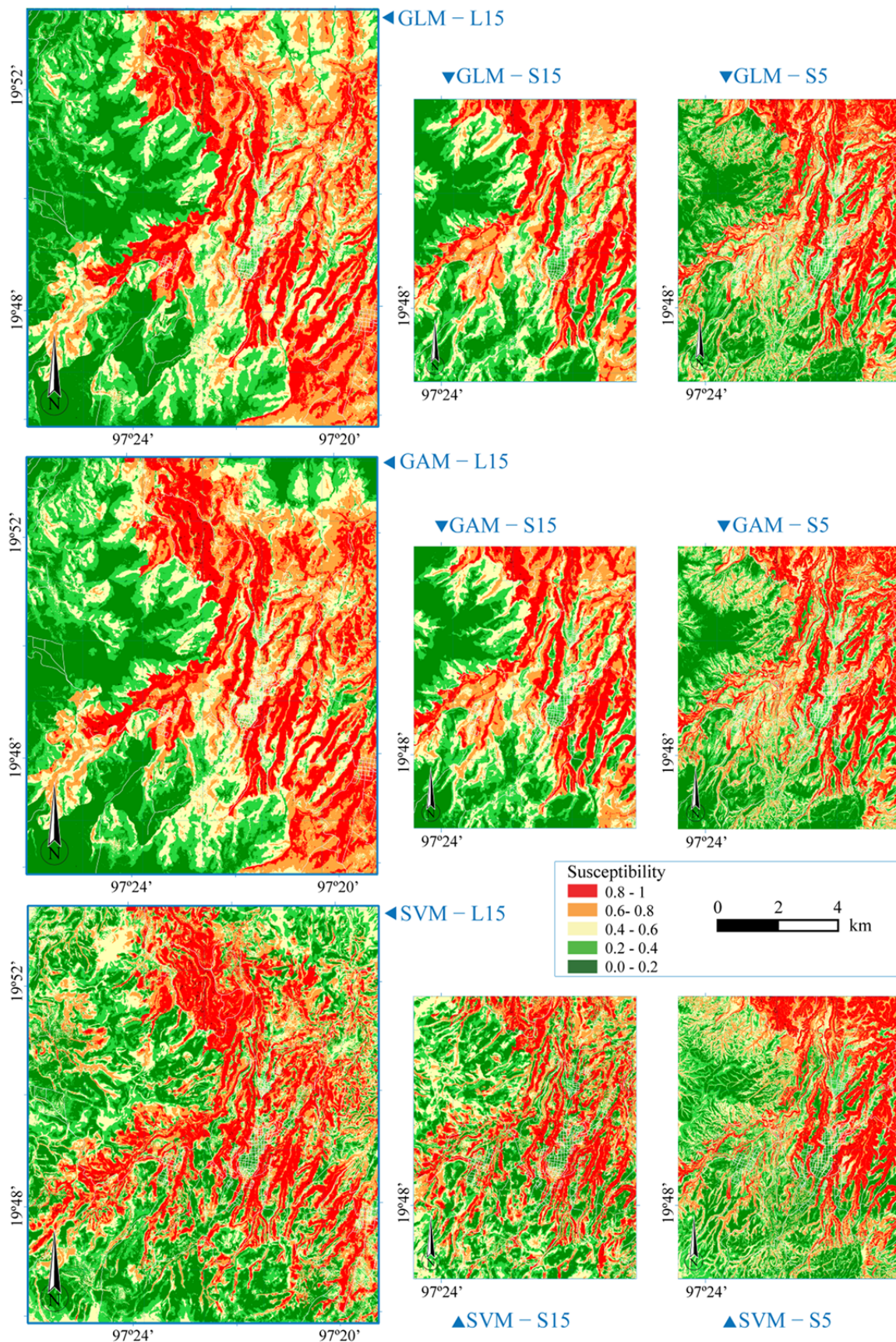


Figure 6 Comparison of predictive surface of landslide susceptibility maps.

scaled thematic information (e.g. Lithology) (Petschko et al. 2014; Steger et al. 2016a). It is assumed that the produced models based on a lower spatial resolution (15 m pixel size) are likely to relate more accurately to the topographic circumstances before slope failure (pre-failure morphology) and thus are more suitable to describe susceptible terrain which was not yet affected by slope instability. In contrast, modelling with higher resolutions bears the danger of training the models towards a too detailed description of past landslide morphology (i.e. performing landslide detection instead of spatial prediction) (van Den Eeckhaut et al. 2006; van Westen et al. 2008; Petschko et al. 2014; Steger et al. 2016b).

Recent landslide susceptibility studies highlighted that a change in the study area delineation can result in rather dissimilar prediction patterns within the identical sub-region and divergent model performance estimates (Gordo et al. 2017; Steger and Glade 2017). The conducted visual confrontation of landslide susceptibility patterns that were based on different study area extents (but identical raster resolution and classifiers) only partly confirmed these previous observations. Compared to these previous studies, differences were not as evident, also because the enlargement of the areal extent (i.e. from data set S15 to L15) was not associated with an inclusion of a high portion of unsusceptible (e.g. flat) and easy to classify terrain. In fact, observed similar predictive performance estimates among the models associated with the data sets L15 and S15 provided quantitative evidence that the classification task (i.e. discriminating landslide presences from absences) has not been facilitated substantially by simply changing the study area extent.

Another point worth further consideration relates to the selection of a suitable set of explanatory variables. Land cover was a-priori excluded from modeling procedure to avoid a direct propagation of an expected land-cover related landslide mapping bias (cf. section 2.2) into the final modeling results (Steger et al. 2017). Within this study, environmental factors were chosen heuristically (Kavzoglu et al. 2015) in order to take advantage of extensive field experiences (Murillo-García and Alcántara-Ayala 2017) and to reduce the danger of obtaining systematically

distorted modelling results (Steger et al. 2016a). Despite a careful evaluation of input data, lack of detailed information on soil properties poses a major drawback of this study, given that the importance of near surface underground conditions observed during field surveys. It is expected that the included lithology layer can just partly be seen as a useful proxy for subsurface conditions, even though this variable contributed substantially to “predict” test set data (i.e. the AUROC increased from 0.684-0.766 to 0.759-0.817 by including lithology).

Other selected thematic variables, such as the distance to spring or the distance to streams, are as well known to not fully represent the influence of linear and punctual water supply. However, field surveys as well as a positive influence of the present spatial data sets on predictive performance estimates supported their inclusion within the models.

K-fold cross validation indicated that the models performed “acceptably well” to “excellent” (Hosmer and Lemeshow 2000) to spatially discriminate independent test data, with higher performances scores for more flexible modelling algorithms. However, it is also known that predictive performance estimates “solely” depict the degree of match between the predicted probability scores and independent test data (Chung and Fabbri 2003; Guzzetti et al. 2006). The sole evaluation of predictive performances of models associated with identical input data suggests that GLMs were outperformed by the GAMs while SVMs constantly perform best.

However, the inspection of the calculated model overfitting scores also highlights that an increasing flexibility of the modelling algorithm was accompanied by an increasing degree of model overfitting. “Overlearning” might be a particular problem in the context of omnipresent error-prone data sets, due to the higher potential to model not only geomorphic plausible relationships, but also input data flaws (Steger et al. 2016b; Steger et al. 2017). The holistic evaluation of the modelling results revealed that the selection of the “best” model for an area is a challenging task and should not be driven by the interpretation of a single performance metric (Rossi et al. 2010; Reichenbach et al 2018). Future analyses based on a spatial cross validation framework are expected

to allow deeper insights into both, model uncertainties and the relevance of predictor variables within a multiple variable modelling context (Schratz et al. 2018).

In synthesis, the map produced with SVM for the data set L15 (Figure 7) was selected to be most

suitable for the purpose of this study. This choice was strongly influenced by obtained predictive performance estimates, the covered areal extent (i.e. the map covers the entire study site) while simultaneously providing a slightly higher spatial differentiation of predicted susceptibility scores (i.e.

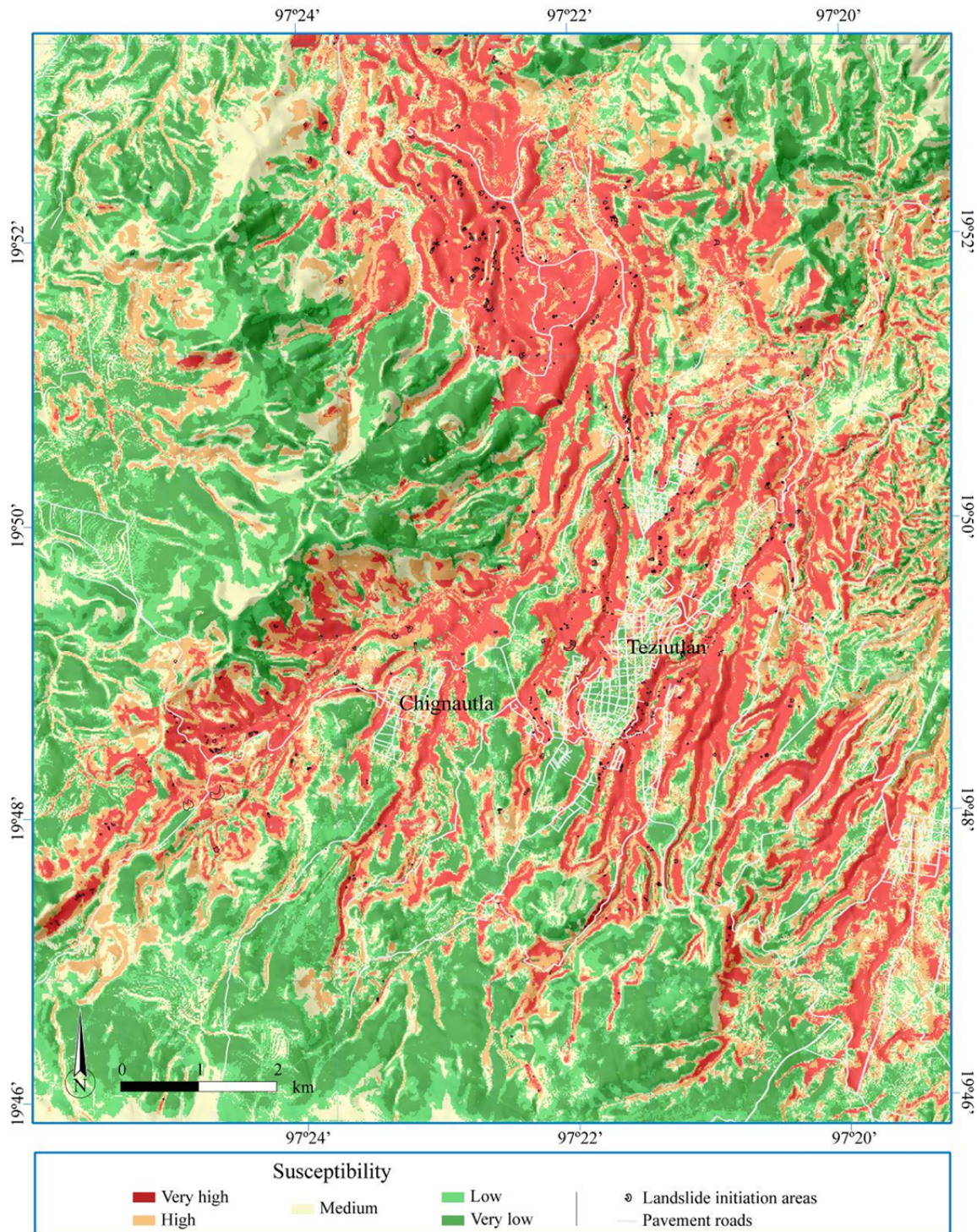


Figure 7 Landslide susceptibility map for data set L15 based on the SVM classifier and underlain by a shaded relief image.

in comparison to GLM and GAM). The major drawback of this selection can be associated to the comparably high degree of model overfitting. Given that past landslide locations of the area are likely to be reactivated in the future, the detected model overfitting was not judged to be a major drawback in the context of this study.

For the study area, elevation can be associated with lithology: highest elevations are in the Southwest (where the LHCV is located) and in Chignautla hill. In the Southwest portion, characterised by the presence of basalt lava flows and consolidated ignimbrite, number of landslide occurrence is low. Additionally, in Chignautla hill (composed mainly by sedimentary hard rocks) landslide occurrence is not that high either. In all the produced maps is clear that low and very low susceptibility values are predominate at the South and West areas. In contrast, in the North and Southeast sectors of the study area (with minor elevation values), where the ramp of unconsolidated pyroclastic deposits is situated (see [Murillo-García and Alcántara-Ayala 2017](#)), landslide occurrence is higher. Besides, the high capacity of water retention of the unconsolidated volcanic materials and soils of the pyroclastic ramp suggest that these materials are prone to landslides occurrence. Although the top of the pyroclastic ramp cannot be considered as a plain surface, in all maps the top of the pyroclastic ramp shows low and very low susceptibility values. In the other hand, landslides occur mainly at the slopes of ravines of the pyroclastic ramp. In all the nine susceptibility maps these slopes exhibit high and very high values. An issue to take into account, is that the urban growth of Teziutlán town (intensified in the second half of the 20th century) made that the slopes of the pyroclastic ramp where occupied to build new households (this is similar for Chignautla town).

5 Conclusions

A data-driven landslide susceptibility analysis was carried out for an area where sedimentary rocks are overlaid by a ramp formed by unconsolidated pyroclastic and fall volcanic deposits. Besides two different study area extents (L vs. S), two different DEMs with pixel sizes of 5 m

(only available for the smaller S region) and 15 m were tested in order to produce three different modelling data sets (L15 15 m, S5 5 m, S15 15 m). Furthermore, three differently flexible binary soft classification algorithms were tested using logistic regression (GLM), general additive modelling (GAM) and support vector machine (SVM).

The conducted expert-based selection of explanatory variables took also into account the results of an exploratory data analysis, such as the evaluation of a variables individual classification power. The selected explanatory variables were slope angle, aspect, lithology, relative slope position, elevation, convergence index, distance to streams, distance to springs and topographic wetness index. Each model has been evaluated by repeatedly splitting the initial data into multiple training and test sets within a k-fold cross validation framework.

The final model selection was guided by the AUROC scores (i.e. highest median AUROC: 0.82), the covered areal extent (i.e. largest areal coverage) and the spatial pattern of the predicted landslide susceptibility scores. The results revealed that a higher modelling resolution does not necessarily favour better performing models. It was highlighted that differences in the modelling results (e.g. prediction patterns) were determined by an interplay of selected classification algorithm, study area delineation and pixel resolution. The most suitable model for the purpose of this study was produced with the comparably flexible SVM classifier. Finally, it is suggested that the selection of best models should not be based only on an interpretation of obtained model prediction skills, since many non-quantifiable aspects co-determine the explanatory power and usability of modelling results.

Acknowledgements

Authors from UNAM gratefully acknowledge the financial support provided by CONACyT and DGAPA-UNAM PAPIIT through the Research Projects 156242 and IN300818, respectively. Special thanks also to CONACyT for granting a PhD scholarship and to Federica Fiorucci from CNR-IRPI Perugia, Italy, for supporting the generation of the landslide inventory.

References

- Akgün A, Bulut F (2007) GIS-based landslide susceptibility for Arsin-Yomra (Trabzon, North Turkey) region. *Environmental Geology* 51:1377-1387. <https://doi.org/10.1007/s00254-006-0435-6>
- Althuwaynee OF, Pradhan B, Park HJ, Lee JH (2014) A novel ensemble bivariate statistical evidential belief function with knowledge-based analytical hierarchy process and multivariate statistical logistic regression for landslide susceptibility mapping. *Catena* 114: 21-36. <https://doi.org/10.1016/j.catena.2013.10.011>
- Ardizzone F, Cardinali M, Carrara A, et al. (2002) Impact of mapping errors on the reliability of landslide hazard maps. *Natural Hazards and Earth System Science* 2: 3-14. <https://doi.org/10.5194/nhess-2-3-2002>
- Atkinson PM, Massari R (1998) Generalised linear modelling of susceptibility to landsliding in the central Apennines, Italy. *Computers & Geosciences* 24(4): 373-385. [https://doi.org/10.1016/S0098-3004\(97\)00117-9](https://doi.org/10.1016/S0098-3004(97)00117-9)
- Ayalew L, Yamagishi H, Ugawa N (2004) Landslide susceptibility mapping using GIS-based weighted linear combination, the case in Tsugawa area of Agano River, Niigata Prefecture, Japan. *Landslides* 1: 73-81. <https://doi.org/10.1007/s10346-003-0006-9>
- Beven KJ, Kirkby MJ (1979) A physically based, variable contributing area model of basin hydrology. *Hydrology Science Bulletin* 24: 43-69.
- Bischl B, Lang M, Kothhoff L, et al. (2016) mlr: Machine Learning in R. R package version 2.9. <https://CRAN.R-project.org/package=mlr>
- Brabb EE (1984) Innovative approaches to landslide hazard mapping. *Proceedings 4th International Symposium on Landslides, Toronto* 1: 307-324.
- Brenning A (2005) Spatial prediction models for landslide hazards: review, comparison and evaluation. *Natural Hazards and Earth System Science* 5: 853-862. <https://doi.org/10.5194/nhess-5-853-2005>
- Brenning A (2008) Statistical geocomputing combining R and SAGA: the example of landslide susceptibility analysis with generalized additive models. In: Böhner J, Blaschke T, Montanarella L (eds.), *SAGA – Seconds Out (= Hamburger Beiträge zur Physischen Geographie und Landschaftsökologie, 19)*. pp 23-32.
- Brenning A (2012) Spatial cross-validation and bootstrap for the assessment of prediction rules in remote sensing: the R package 'sperrrest'. *IEEE International Symposium on Geoscience and Remote Sensing IGARSS*. <https://ieeexplore.ieee.org/document/6352393>
- Capra L, Lugo-Hubp J, Borselli L (2003) Mass movements in tropical volcanic terrains: the case of Teziutlán (Mexico). *Engineering Geology* 69: 359-379. [https://doi.org/10.1016/S0013-7952\(03\)00071-1](https://doi.org/10.1016/S0013-7952(03)00071-1)
- Cardinali M, Reichenbach P, Guzzetti F, et al. (2002) A geomorphological approach to estimate landslide hazard and risk in urban and rural areas in Umbria, central Italy. *Natural Hazards and Earth System Science* 2 (1-2): 57-72. <https://www.nat-hazards-earth-syst-sci.net/2/57/2002/nhess-2-57-2002.pdf>
- Cascini L (2008) Applicability of landslide susceptibility and hazard zoning at different scales. *Engineering Geology* 102: 164-177. <https://doi.org/10.1016/j.enggeo.2008.03.016>
- Catani F, Lagomarsino D, Segoni S, Tofani V (2013) Landslide susceptibility estimation by random forests technique: sensitivity and scaling issues. *Natural Hazards and Earth System Science* 13: 2815-2831. <https://doi.org/10.5194/nhess-13-2815-2013>
- Chauhan S, Sharma M, Arora MK (2010) Landslide susceptibility zonation of the Chamoli region, Garhwal Himalayas, using logistic regression model. *Landslides* 7:411-423. <https://doi.org/10.1007/s10346-010-0202-3>
- Che VB, Kervyn M, Suh CE, et al. (2012) Landslide susceptibility assessment in Limbe (SW Cameroon): A field calibrated seed cell and information value method. *Catena* 92: 83-98. <https://doi.org/10.1016/j.catena.2011.11.014>
- Chen CH, Ke CC, Huang CL (2009) A back-propagation network for the assessment of susceptibility to rock slope failure in the eastern portion of the Southern Cross-Island Highway in Taiwan. *Environmental Geology* 57: 723-733. <https://doi.org/10.1007/s00254-008-1350-9>
- Chung CJF, Fabbri AG (2003) Validation of spatial prediction models for landslide hazard mapping. *Natural Hazards* 30(3): 451-472. <https://doi.org/10.1023/B:NHAZ.0000007172.62651.2b>
- Chung CF, Fabbri A, Van Westen CJ (1995) Multivariate regression analysis for landslide hazard zonation. In: Carrara A, Guzzetti F (eds.), *Geographical Information Systems in Assessing Natural Hazards* 107-133.
- Conforti M, Pascale S, Robustelli G, Sdao F (2014) Evaluation of prediction capability of the artificial neural networks for mapping landslide susceptibility in the Turbolo River catchment (northern Calabria, Italy). *Catena* 113: 236-250. <https://doi.org/10.1016/j.catena.2013.08.006>
- Conrad O (2006) SAGA - Program structure and current state implementation. In: Böhner J, McCloy KR, Strobl J (eds.), *SAGA – Analysis and Modelling Applications*, vol.115. Göttinger Geographische Abhandlungen. pp 39-52.
- Costanzo D, Rotigliano E, Irigaray C, et al. (2012) Factors selection in landslide susceptibility modelling on large scale following the gis matrix method: application to the river Beiro basin (Spain). *Natural Hazards and Earth System Science* 12: 327-340. <https://doi.org/10.5194/nhess-12-327-2012>
- Dahal RK, Hasegawa S, Nonomura A, et al. (2008) GIS-based weights-of-evidence modelling of rainfall-induced landslides in small catchments for landslide susceptibility mapping. *Environmental Geology* 54(2):314-324. <https://doi.org/10.1007/s00254-007-0818-3>
- Dávila-Harris P, Carrasco-Núñez G (2014) An unusual syn-eruptive bimodal eruption: The Holocene Cuicuiltic Member at Los Humeros caldera, Mexico. *Journal of Volcanology and Geothermal Research* 271: 24-42. <https://doi.org/10.1016/j.jvolgeores.2013.11.020>
- Deb SK, El-Kadi AI (2009) Susceptibility assessment of shallow landslides on Oahu, Hawaii, under extreme-rainfall events. *Geomorphology* 108: 219-233. <https://doi.org/10.1016/j.geomorph.2009.01.009>
- Fell R, Corominas J, Bonnard C, et al. (2008) Guidelines for landslide susceptibility, hazard and risk zoning for land-use planning. *Engineering Geology* 102(3-4): 85-98. <https://doi.org/10.1016/j.enggeo.2008.03.022>
- Ferriz H, Mahood G (1984) Eruption rates and compositional trends at Los Humeros volcanic center, Puebla, Mexico. *Journal of Geophysical Research* 89: 8511-8524.
- Fressard M, Thiery Y, Maquaire O (2014) Which data for quantitative landslide susceptibility mapping at operational scale? Case study of the Pays d'Auge plateau hillslopes (Normandy, France). *Natural Hazards and Earth System Science* 14(3): 569-588. <https://doi.org/10.5194/nhess-14-569-2014>
- Glade T, Crozier M (2005) A review of scale dependency in landslide hazard and risk analysis. In: Glade T, Anderson M, Crozier M (eds) *Landslide hazard and risk*. John Wiley and Sons. England. pp 75-138.
- Goetz JN, Guthrie RH, Brenning A (2011) Integrating physical

- and empirical landslide susceptibility models using generalized additive models. *Geomorphology* 129(3): 376-386. <https://doi.org/10.1016/j.geomorph.2011.03.001>
- Goetz JN, Brenning A, Petschko H, Leopold P (2015) Evaluating machine learning and statistical prediction techniques for landslide susceptibility modeling. *Computers & Geosciences* 81: 1-11. <https://doi.org/10.1016/j.cageo.2015.04.007>
- Gordo C, Zêzere JL, Marques R (2017) Effects of study area delineation on landslide susceptibility assessment results using statistical methods. 8^o Congresso Nacional de Geomorfologia 95-98.
- Gorum T, Fan X, van Westen CJ, et al. (2011) Distribution pattern of earthquake-induced landslides triggered by the 12 May 2008 Wenchuan earthquake. *Geomorphology* 133 (3-4): 152-167. <https://doi.org/10.1016/j.geomorph.2010.12.030>
- Guzzetti F (2005). *Landslide Hazard and Risk Assessment*. PhD thesis, Bonn University, Bonn, Germany.
- Guzzetti F, Carrara A, Cardinali M, Reichenbach P (1999) Landslide hazard evaluation: a review of current techniques and their application in a multi-scale study, Central Italy. *Geomorphology* 31: 181-216. [https://doi.org/10.1016/S0169-555X\(99\)00078-1](https://doi.org/10.1016/S0169-555X(99)00078-1)
- Guzzetti F, Reichenbach P, Cardinali M, et al. (2005) Probabilistic landslide hazard assessment at the basin scale. *Geomorphology* 72: 272-299. <https://doi.org/10.1016/j.geomorph.2005.06.002>
- Guzzetti F, Reichenbach P, Ardizzone F, et al. (2006) Estimating the quality of landslide susceptibility models, *Geomorphology* 81(1-2): 166-184. <https://doi.org/10.1016/j.geomorph.2006.04.007>
- Hastie T (2009) GAM: Generalized Additive Models R package version 1.08. <https://CRAN.R-project.org/package=gam>
- Hastie T, Tibshirani R (1986) *Generalized Additive Models*, *Statistical Science* 1(3): 297-318.
- Hastie TJ, Tibshirani RJ (1990) *Generalized Additive Models*, 1st ed., *Monographs on statistics and applied probability* 43. Chapman and Hall/CRC, London; New York.
- Heckmann T, Gregg K, Gregg A, Becht M (2014) Sample size matters: investigating the effect of sample size on a logistic regression susceptibility model for debris flows. *Natural Hazards and Earth System Science* 14: 259-278. <https://doi.org/10.5194/nhess-14-259-2014>
- Hosmer DW, Lemeshow S (2000) *Applied logistic regression*, 2nd edn. Wiley, New York. pp 373.
- Hong H, Pradhan B, Xua C, Tien Bui D (2015) Spatial prediction of landslide hazard at the Yihuang area (China) using two-class kernel logistic regression, alternating decision tree and support vector machines. *Catena* 133: 266-281. <https://doi.org/10.1016/j.catena.2015.05.019>
- Hussin H, Zumpano V, Reichenbach P, et al. (2016) Different landslide sampling strategies in a grid-based bi-variate statistical susceptibility model. *Geomorphology* 253: 508-523. <https://doi.org/10.1016/j.geomorph.2015.10.030>
- INEGI (2009) *Prontuario de información geográfica municipal de los Estados Unidos Mexicanos*. Teziutlán, Puebla. Instituto Nacional de Geografía y Estadística. p 9. (In Spanish).
- INEGI (2013a) *Continuo de Elevaciones Mexicano 3.0 (CEM 3.0) - descarga Antecedentes*. Available online at: <http://www.inegi.org.mx/geo/contenidos/datosrelieve/continuo/continuoelevaciones.aspx> (Accessed on 08 August 2018) (In Spanish).
- INEGI (2013b) *Modelo digital de elevación de alta resolución LiDAR, Tipo terreno con resolución de 5 m*. Available online at: <http://www.inegi.org.mx/est/contenidos/proyectos/Preview.aspx> (Accessed on 08 August 2018) (In Spanish).
- Karatzoglou A, Smola A, Hornik K, Zeileis A (2004) *Kernlab - An S4 Package for Kernel methods in R*. *Journal of Statistical Software* 11(9): 1-20. <http://www.jstatsoft.org/v11/i09/>
- Kavzoglu T, Sahin EK, Colkesen I (2014) Landslide susceptibility mapping using GIS-based multicriteria decision analysis, support vector machines, and logistic regression. *Landslides* 11: 425-439. <https://doi.org/10.1007/s10346-013-0391-7>
- Kavzoglu T, Sahin EK, Colkesen I (2015) Selecting optimal conditioning factors in shallow translational landslide susceptibility mapping using genetic algorithm. *Engineering Geology* 192: 101-112. <https://doi.org/10.1016/j.enggeo.2015.04.004>
- Kotsiantis SB (2007) *Supervised Machine Learning: A Review of Classification Techniques*. *Informatica* 31, 249-268.
- Lee S, Choi J, Woo I (2004) The effect of spatial resolution on the accuracy of landslide susceptibility mapping: a case study in Boun, Korea. *Geoscience Journal* 8: 51-60. <https://doi.org/10.1007/BF02910278>
- Legorreta-Paulín, Bursik M, Lugo-Hubp J, Zamorano-Orozco JJ (2010) Effect of pixel size on cartographic representation of shallow and deep-seated landslide, and its collateral effects on the forecasting of landslides by SINMAP and Multiple Logistic Regression landslide models. *Physics and Chemistry of the Earth* 35: 137-148. <https://doi.org/10.1016/j.pce.2010.04.008>
- Moore ID, Grayson RB, Ladson AR (1991) Digital terrain modeling: a review of hydrological, geomorphological, and biological applications. *Hydrological Process* 5: 3-30. <https://doi.org/10.1002/hyp.3360050103>
- Murillo-García FG, Alcántara-Ayala I (2017) *Landslide inventory, Teziutlán municipality, Puebla, México (1942-2015)*. *Journal of maps* 13(2): 767-776. <https://doi.org/10.1080/17445647.2017.1381194>
- Olaya V (2004) *A Gentle Introduction to SAGA GIS*. ftp://priede.bf.luv/pub/GIS/datu_analize/SAGA/SagaManual.pdf
- Palamakumbure D, Flentje P, Stirling D (2015) Consideration of optimal pixel resolution in deriving landslide susceptibility zoning within the Sydney Basin, New South Wales, Australia. *Computers & Geosciences* 82: 13-22. <https://doi.org/10.1016/j.cageo.2015.05.002>
- Park NW, Chi KH (2008) Quantitative assessment of landslide susceptibility using high-resolution remote sensing data and a generalized additive model. *International Journal of Remote Sensing* 29: 247-264. <https://doi.org/10.1080/01431160701227661>
- Petschko H, Bell R, Leopold P, et al. (2013) *Landslide inventories for reliable susceptibility maps*. In: Margottini C, Canuti P, Sassa K (Eds.), *Landslide Science and Practice*, vol. 1: *Landslide Inventory and Susceptibility and Hazard Zoning*. Springer.
- Petschko H, Brenning A, Bell R, et al. (2014) Assessing the quality of landslide susceptibility maps - case study Lower Austria *Natural Hazards and Earth System Science* 14: 95-118. <http://doi.org/10.5194/nhess-14-95-2014>
- Petschko H, Bell R, Glade T (2016) Effectiveness of visually analyzing LiDAR DTM derivatives for earth and debris slide inventory mapping for statistical susceptibility modelling. *Landslides* 13 (5): 857-872. <https://doi.org/10.1007/s10346-015-0622-1>
- Pourghasemi HR, Rahmati O (2018) Prediction of the landslide susceptibility: Which algorithm, which precision? *Catena* 162: 177-192. <https://doi.org/10.1016/j.catena.2017.11.022>
- Pradhan S (2013) A comparative study on the predictive ability of the decision tree, support vector machine and neuro-fuzzy models in landslide susceptibility mapping using GIS. *Computers & Geosciences* 51:350-365. <https://doi.org/10.1016/j.cageo.2012.08.023>
- Qi S, Xu Q, Lan H, et al. (2010) Spatial distribution analysis of landslides triggered by 2008.5.12 Wenchuan Earthquake, China *Engineering Geology* 116 (1-2): 95-108. <http://doi.org/10.1016/j.enggeo.2010.07.011>
- QGIS Development Team (2009) *QGIS Geographic Information System*. Open Source Geospatial Foundation. <http://qgis.osgeo.org>
- R Core Team (2016) *R: A language and environment for statistical computing*. R Foundation for Statistical Computing, Vienna, Austria. <https://www.R-project.org/>
- Regmi NR, Giardino JR, McDonald E, Vittek JD (2014) A

- comparison of logistic regression based models of susceptibility to landslides in western Colorado, USA. *Landslides* 11: 247-262.
<https://doi.org/10.1007/s10346-012-0380-2>
- Reichenbach P, Rossi M, Malamud BD, et al. (2018) A review of statistically-based landslide susceptibility models. *Earth-Science Reviews* 180: 60-91.
<https://doi.org/10.1016/j.earscirev.2018.03.001>
- Romer C, Ferentinou M (2016) Shallow landslide susceptibility assessment in a semiarid environment –A Quaternary catchment of Kwa Zulu-Natal, South Africa. *Engineering Geology* 201: 29-44.
<https://doi.org/10.1016/j.enggeo.2015.12.013>
- Rossi M, Guzzetti F, Reichenbach P, et al. (2010) Optimal landslide susceptibility zonation based on multiple forecasts. *Geomorphology* 114: 129-142.
<https://doi.org/10.1016/j.geomorph.2009.06.020>
- Salinas-Rodríguez JM, Castillo-Reynoso JE (2011) Carta Geológica Minera. Teziutlán E14B15 Puebla. Servicio Geológico Mexicano.
- San BT (2014) An evaluation of SVM using polygon-based random sampling in landslide susceptibility mapping: The Candir catchment area (western Antalya, Turkey). *International Journal of Applied Earth Observation and Geoinformation* 26: 399-412.
- Schlögel R, Marchesini I, Alvioli M, et al. (2018) Optimizing landslide susceptibility zonation: Effects of DEM spatial resolution and slope unit delineation on logistic regression models. *Geomorphology* 301: 10-20.
<https://doi.org/10.1016/j.geomorph.2017.10.018>
- Schratz P, Muenchow J, Iturritxa E, et al. (2018) Performance evaluation and hyperparameter tuning of statistical and machine-learning models using spatial data. *Journal of LATEX Templates*. <https://arxiv.org/abs/1803.11266>
- Sing T, Sander O, Beerenwinkel N, Lengauer T (2009) ROCR: Visualizing the Performance of Scoring Classifiers. R package version 1.0-4. <http://cran.r-project.org/package=ROCR>
- Steger S, Glade T (2017) The Challenge of "Trivial Areas" in Statistical Landslide Susceptibility Modelling. In: Matjaž M et al. (eds.) *Advancing Culture of Living with Landslides WLF 2017*, Springer, Cham. 2: 803-808.
https://doi.org/10.1007/978-3-319-53498-5_92
- Steger S, Brenning A, Bell R, et al. (2016a) Exploring discrepancies between quantitative validation results and the geomorphic plausibility of statistical landslide susceptibility maps. *Geomorphology* 262: 8-23.
<https://doi.org/10.1016/j.geomorph.2016.03.015>
- Steger S, Brenning A, Bell R, Glade T (2016b) The propagation of inventory-based positional errors into statistical landslide susceptibility models. *Natural Hazards and Earth System Science* 16(12): 2729-2745.
<https://doi.org/10.5194/nhess-2016-301>
- Steger S, Brenning A, Bell R, Glade T (2017) The influence of systematically incomplete shallow landslide inventories on statistical susceptibility models and suggestions for improvements. *Landslides* 14:1767-1781.
<https://doi.org/10.1007/s10346-017-0820-0>
- Trigila A, Iadanza C, Esposito C, Scarascia-Mugnozza G (2015) Comparison of Logistic Regression and Random Forests techniques for shallow landslide susceptibility assessment in Giampilieri (NE Sicily, Italy). *Geomorphology* 249: 119-136.
<https://doi.org/10.1016/j.geomorph.2015.06.001>
- Van Den Eeckhaut M, Vanwalleghem T, Poesen J, et al. (2006) Prediction of landslide susceptibility using rare events logistic regression: A case-study in the Flemish Ardennes (Belgium). *Geomorphology* 76(3-4): 392-410.
<https://doi.org/10.1016/j.geomorph.2005.12.003>
- van Westen CJ, Rengers N, Terlien MTJ, Soeters R (1997) Prediction of the occurrence of slope instability phenomena through GIS-based hazard zonation. *Geologische Rundschau* 86: 404-414.
- van Westen CJ, Seijmonsbergen AC, Mantovani F (1999) Comparing landslide hazard maps. *Natural Hazards* 20: 137-158.
- van Westen CJ, Castellanos E, Kuriakose SL (2008) Spatial data for landslide susceptibility, hazard, and vulnerability assessment: An overview. *Engineering Geology* 102(3-4): 112-131. <https://doi.org/10.1016/j.enggeo.2008.03.010>
- Vapnik V (1998) *Statistical Learning Theory*. John Wiley & Sons Inc., New York. p 736.
- Varnes DJ, IAEG Commission on Landslides and other Mass-Movements (1984) *Landslide hazard zonation: a review of principles and practice*. The UNESCO Press, Paris. p 63.
- Vorpahl P, Elsenbeer H, Märker M, Schröder, B (2012) How can statistical models help to determine driving factors of landslides? *Ecol. Model* 239: 27-39.
<https://doi.org/10.1016/j.ecolmodel.2011.12.007>
- Wood SN (2006) Generalized additive models: an introduction with R. Chapman & Hall/CRC, Boca Raton, FL.
- Youssef AM, Pradhan B, Pourghasemi HR, Abdullahi S (2015) Landslide susceptibility assessment at Wadi Jawrah Basin, Jizan region, Saudi Arabia using two bivariate models in GIS. *Geosciences Journal* 19(3): 449-469.
<https://doi.org/10.1007/s12303-014-0065-z>
- Zézere JL, Pereira S, Melo R, et al. (2017) Mapping landslide susceptibility using data-driven methods. *Science of the Total Environment* 589: 250-267.
<https://doi.org/10.1016/j.scitotenv.2017.02.188>
- Zweig MH, Campbell G (1993) Receiver-operating characteristic (ROC) plots. *Clinical Chemistry* 39: 561-577.